Original Research

Thermodynamic compensation indicates binding promiscuity of dystrophin in the nervous system

Madison E. Fountain[1], Sarah F. Cuneio[1], Jonghoon Kang[1 *]

[1]Valdosta State University, Department of Biology, 1500 N Patterson St., Valdosta, Georgia 31698, USA

***Correspondence**: jkang@valdosta.edu
DOI: https://doi.org/10.56280/1723375325

Received: 20 November 2025 Accepted: 27 November 2025 Online Published: 8 December 2025

Abstract

Dystrophin plays a key role in neuronal structure and synaptic signaling, yet its full range of binding partners in the nervous system remains incompletely understood. Here, we examined dystrophin–dystrobrevin interactions using a combined thermodynamic and bioinformatic approach. Analysis of published calorimetric data revealed that binding is driven primarily by favorable electrostatic and polar interactions and displays strong enthalpy–entropy compensation (EEC), with a notably low compensation temperature, suggesting that dystrophin may accommodate diverse partners through compensatory energetics. Bioinformatic profiling and principal component analysis (PCA) distinguished dystrobrevin isoforms and indicated that the C-terminal flanking region and overall charge (pI) are key determinants of binding affinity. Multiple linear regression further showed that $\Delta G°$ can be predicted from sequence-derived variables, particularly pI and intrinsic disorder. Together, these findings provide a thermodynamic rationale for the broad interaction capacity of dystrophin and establish a sequence-based framework for identifying potential dystrophin-binding proteins in the nervous system.

Keywords: *dystrophin; dystrobrevin; enthalpy–entropy compensation; coiled-coil interactions; principal component analysis; multiple linear regression*

1. Introduction

Protein–protein interactions (PPIs) are fundamental to neuronal structure and signaling, organizing synaptic scaffolds, receptor clusters, and signaling microdomains across the brain. Disruption of these interaction networks is increasingly implicated in neurodevelopmental, psychiatric, and neurodegenerative disorders (Dang et al., 2025; Howes et al., 2025; Mathew et al., 2022; Matsubayashi & Takano, 2025).

Dystrophin, best known for its mechanical role in muscle, also forms specialized scaffolds in the nervous system via brain isoforms (e.g., Dp71), where it helps organize $GABA_A$ receptors and other synaptic components; loss of dystrophin perturbs inhibitory signaling and is linked to cognitive and seizure phenotypes in Duchenne muscular dystrophy (Naidoo & Anthony, 2020; Sekiguchi et al., 2009). Within the dystrophin-associated protein complex (DAPC), dystrophin engages dystrobrevin and syntrophins through coiled-coil interactions, creating a structural-signaling hub at membranes (Peters et al., 1997). Although many interactors of dystrophin and dystrobrevin have been identified, including isoform-specific partners and additional coiled-coil–binding proteins (e.g., dysbindin), the brain/DAPC interactome continues to expand and appears tissue- and isoform-specific, suggesting the current list is incomplete (Benson et al., 2001; Roberts, 2001).

Enthalpy–entropy compensation (EEC) provides a quantitative framework to understand "promiscuous" binding: across related complexes or perturbations, favorable enthalpy can trade off against unfavorable entropy (and vice-versa) while maintaining similar free energies (Fox et al., 2018). EEC has been linked to interaction promiscuity in protein systems, including intrinsically disordered and multi-partner complexes, and offers a thermodynamic lens to infer broad specificity, which is consistent with our and others previous analyses (Durrani & Kang, 2020; Kang & Kang, 2021; Kang & Smidtas, 2021; Kragelj et al., 2021).

Journal of Multiscale Neuroscience

Recently, biophysical work on the dystrophin C-terminal (CT) domain demonstrated that dystrophin binds dystrobrevin isoforms via intermolecular coiled-coils, with measurable binding thermodynamics that differ between isoforms, providing an ideal dataset to test for EEC in dystrophin-mediated interactions (Upadhyay et al., 2024). In the present paper, we show our analysis of dystrophin–dystrobrevin interactions to identify EEC in the interactions.

2. Materials and methods

2.1 System of study

The original study characterized the interaction between the C-terminal domain of dystrophin (Dys-CT) and the coiled-coil motifs of different dystrobrevin isoforms. Two native dystrobrevin constructs were analyzed: DBNa-CC (the coiled-coil region of dystrobrevin-α) and DBNb-CC (the coiled-coil region of dystrobrevin-β). To investigate the contribution of flanking sequence elements, two engineered variants of DBNb-CC were also examined. DBNb-CC-NTM: DBNb-CC in which the first nine amino acids were replaced with the corresponding N-terminal segment from DBNa-CC. DBNb-CC-CTM: DBNb-CC in which the last seventeen amino acids were replaced with the corresponding C-terminal segment from DBNa-CC. These substitutions allowed the systematic evaluation of how N-terminal and C-terminal flanking regions influence coiled-coil energetics and binding thermodynamics. Multiple sequence alignment of all dystrobrevin variants was performed using the Clustal Omega algorithm (EMBL-EBI; https://www.ebi.ac.uk/jdispatcher/msa/clustalo).

2.2 Thermodynamic characterization and enthalpy–entropy compensation

Thermodynamic properties of the dystrophin–dystrobrevin interactions were analyzed using the reported means and standard deviations of the four binding reactions. The standard free energy change ($\Delta G°$) at 37 °C was calculated from the enthalpy ($\Delta H°$) and entropy ($\Delta S°$) changes using Eq. (1):

$$\Delta G° = \Delta H° - T\Delta S° \quad (1)$$

where T is the absolute temperature in Kelvin (Chang, 2000). A linear positive correlation between $\Delta H°$ and $\Delta S°$ across a series of related binding reactions is defined as enthalpy–entropy compensation (EEC) (Fox et al., 2018). The presence of EEC was tested among the four dystrophin–dystrobrevin interactions using linear regression, following Eq. (2):

$$\Delta H° = T_C \Delta S° + \beta \quad (2)$$

where T_C is the compensation temperature (the slope of the regression line), and β is the y-intercept (Daune, 1999; Griessen & Dam, 2021). Outlier detection was performed using the studentized deleted residual method. Data points with studentized deleted residuals < –2.5 or > 2.5 were classified as statistical outliers (Pardoe, 2012; Kang & Kang, 2021).

2.3 Multivariate statistical analysis of bioinformatic data

Dystrobrevin isoforms and their engineered variants were evaluated for several bioinformatic properties (Payá et al., 2023), including isoelectric point (pI), aliphatic index (AI), grand average of hydropathy (GRAVY), average flexibility (AF), and average disorder (AD). The first three parameters (pI, AI, and GRAVY) were obtained from the ExPASy ProtParam portal (https://web.expasy.org/protparam/). AF values were computed using the ExPASy ProtScale tool (https://web.expasy.org/protscale/). Average disorder estimates were obtained from IUPred3 (https://iupred3.elte.hu/), using the long-disorder option with medium smoothing.

Principal component analysis (PCA) was performed using the five bioinformatic variables in combination with the standard free energy change ($\Delta G°$) at 37 °C. Because the variables represent heterogeneous scales and units, the correlation matrix was used as the basis for PCA.

Multiple linear regression (Roustaei, 2024) was conducted according to Eq. (3):

$$\Delta G°(37\ °C) = a_1 x_1 + a_2 x_2 + c \quad (3)$$

where a_1, a_2, and c are regression coefficients, and x_1 and x_2 correspond to two most informative variables identified through PCA. Only two predictors were used because the dataset consisted of four data points. All statistical analyses were performed using SigmaPlot (version 15, Grafiti LLC, Palo Alto, CA).

```
DBNa-CC          SAPDISFTIDANKQQRQLIAELENKNREILQEIQRLRLEHEQASQPTPEKAQQNPTLLAE   60
DBNb-CC          PPTDLSFNFDANKQQRQLIAELENKNREILQEIQRLRLEHEQASQPTPEKAQQNPTLLAE   60
DBNb-CC-NTM      SAPDISFTIDANKQQRQLIAELENKNREILQEIQRLRLEHEQASQPTPEKAQQNPTLLAE   60
DBNb-CC-CTM      PPTDLSFNFDANKQQRQLIAELENKNREILQEIQRLRLEHEQASQPTPEKAQQNPTLLAE   60
                    *:**.:**************************************************

DBNa-CC          LRLLRQRKDELEQRMSALQESRRELMVQLEGLMKLLKTQGA-------GSPRSS   107
DBNb-CC          LRLLRQRKDELEQRMSALQESRRELMVQLEELMKLLKEEEQKQAAQATGSPHTS   114
DBNb-CC-NTM      LRLLRQRKDELEQRMSALQESRRELMVQLEELMKLLKEEEQKQAAQATGSPHTS   114
DBNb-CC-CTM      LRLLRQRKDELEQRMSALQESRRELMVQLEELMKLLKTQGA-------GSPRSS   107
                 **************************** ****** :         ***::*
```

Figure 1. *Multiple sequence alignment of four dystrobrevin constructs. The alignment highlights conserved and variable regions among DBNa-CC, DBNb-CC, DBNb-CC-NTM, and DBNb-CC-CTM. Symbols denote the degree of positional conservation: an asterisk (*) indicates identical residues across all sequences; a colon (:) indicates strongly conserved substitutions; and a period (.) denotes weak similarity.*

3. Results

We analyzed the interactions between dystrophin and the four dystrobrevin variants (**Figure 1**) using a thermodynamic framework. To evaluate the presence of EEC, we performed a linear regression of $\Delta H°$ versus $\Delta S°$ using Eq. (2) (**Figure 2a**). The regression revealed a strong linear correlation between $\Delta H°$ and $\Delta S°$ (R^2 = 0.988), clearly demonstrating that dystrophin–dystrobrevin binding follows EEC behavior (**Figure 2a**). No statistical outliers were identified by the studentized deleted residual test. The fitted parameters yielded a T_C of 215 ± 17 K and β of –8.85 ± 0.26 kcal/mol. Notably, the T_C value is substantially lower than previously reported values for protein–peptide interactions, 308.4 ± 6.6 K (Kang & Smidtas, 2021) or for DNA–quercetin binding, 297.3 ± 3.8 K, (Taylor et al., 2023). To our knowledge, this is the first demonstration of EEC in dystrophin–dystrobrevin interactions. These results suggest that EEC may be a general feature of dystrophin-mediated binding and examining additional dystrophin–dystrobrevin pairings—or other dystrophin interaction partners—may further clarify whether thermodynamic compensation contributes to the broad binding promiscuity characteristic of dystrophin's interactome (Kang & Smidtas, 2021).

The mean and standard deviation values of $\Delta H°$, $T\Delta S°$, and $\Delta G°$ at 37 °C are summarized in the bar plot (**Figure 2b**). The plot shows that dystrophin–dystrobrevin binding is driven primarily by favorable enthalpic contributions, whereas the entropic term is consistently unfavorable. This pattern suggests that hydrogen bonding and electrostatic interactions dominate the binding mechanism (Kang & Auerbach, 2009), while hydrophobic effects contribute minimally (Chang, 2000). The standard deviations of $\Delta H°$ and $T\Delta S°$ across the four interactions are approximately three-fold and two-fold larger, respectively, than that of $\Delta G°$ (**Figure 2b**). This disparity reflects the characteristic behavior of EEC, in which variations in $\Delta H°$ and $\Delta S°$ largely cancel, yielding relatively constant free energy values.

Bioinformatic characteristics of the dystrobrevin isoforms and their mutants are summarized in **Table 1**. The pI of DBNa-CC is above 7, indicating that it is a basic protein and would carry a net positive charge at physiological pH. In contrast, the dystrophin sequence used in the binding experiments has a pI of 5.11 (data not shown), consistent with an acidic protein carrying

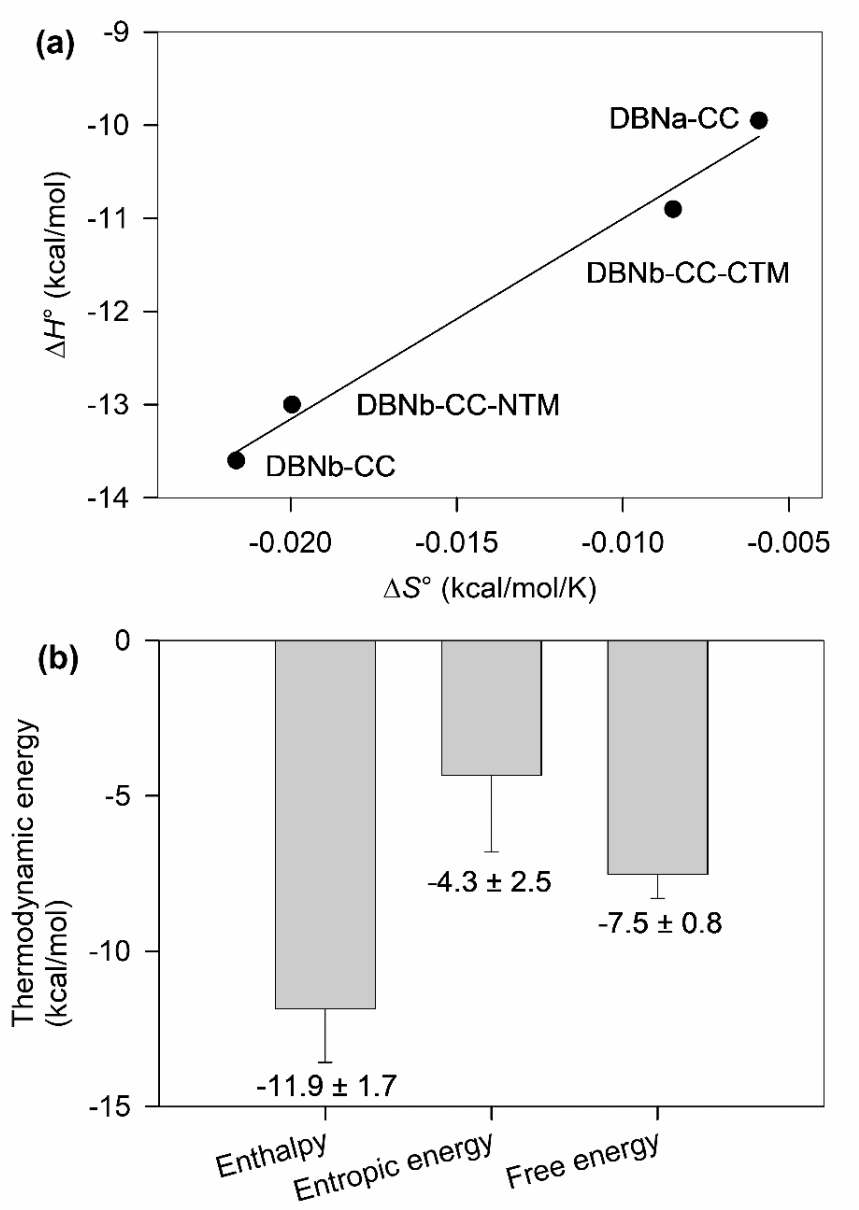

Figure 2. *Thermodynamic characterization of dystrophin–dystrobrevin binding. (a) EEC plot for the four dystrobrevin constructs binding to the dystrophin C-terminal domain. Standard enthalpy changes (ΔH°) are plotted against standard entropy changes (ΔS°). A strong linear correlation (R^2 = 0.988) indicates clear EEC behavior across DBNa-CC, DBNb-CC, DBNb-CC-NTM, and DBNb-CC-CTM. The fitted line yields a compensation temperature of 215 ± 17 K. (b) Mean thermodynamic energies (± SD) across the four dystrophin–dystrobrevin interactions at 37 °C. Binding is driven by favorable enthalpy (–11.9 ± 1.7 kcal/mol) and opposed by unfavorable entropic contributions (–4.3 ± 2.5 kcal/mol), resulting in an overall free energy of –7.5 ± 0.8 kcal/mol. The pattern demonstrates partial cancellation of ΔH° and TΔS°, consistent with EEC.*

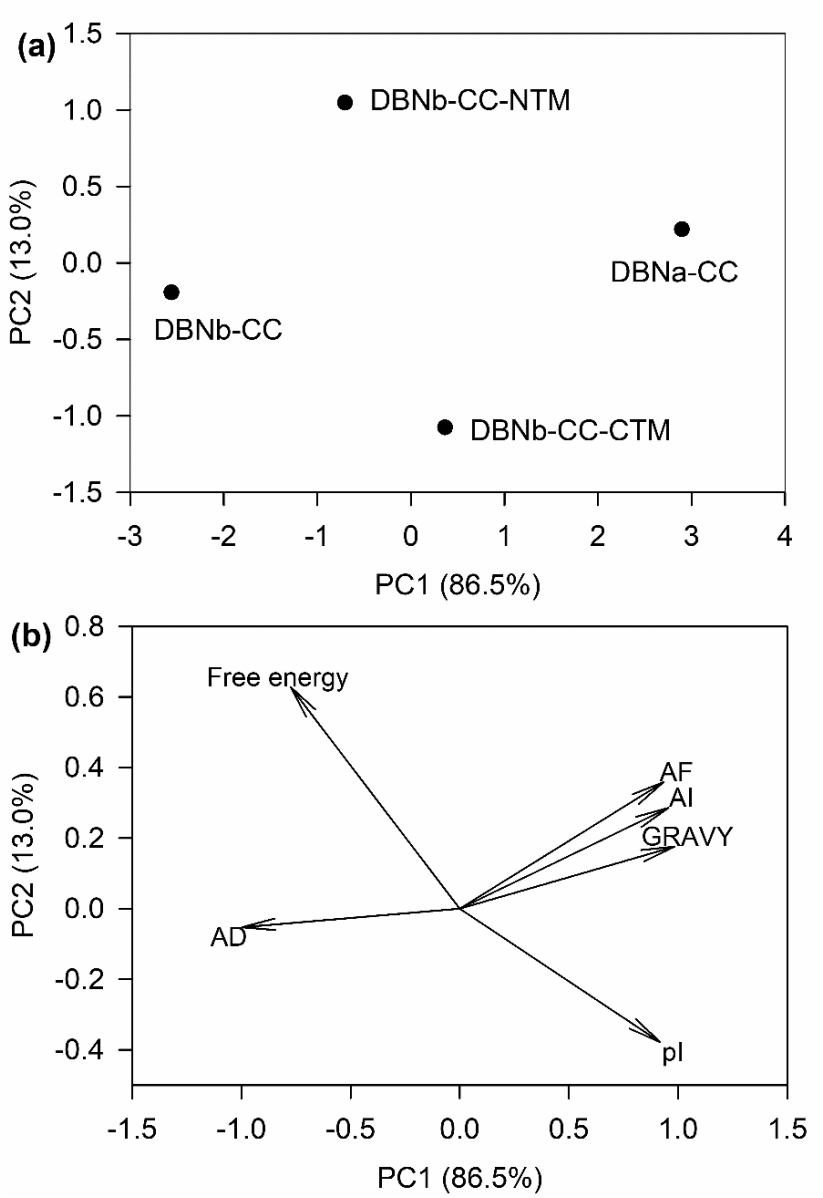

Figure 3. *PCA of dystrobrevin variants and sequence-derived variables. (a) Score plot of the first two principal components (PC1 and PC2), which together explain 99.5% of the total variance (PC1: 86.5%; PC2: 13.0%). PC1 clearly separates the two dystrobrevin isoforms (DBNa-CC and DBNb-CC). The N-terminal mutant DBNb-CC-NTM clusters near DBNb-CC along PC1, whereas the C-terminal mutant DBNb-CC-CTM shifts toward DBNa-CC, indicating that the C-terminal flanking region contributes strongly to the physicochemical properties relevant to dystrophin binding. (b) Loadings plot showing the contributions of the six variables (ΔG°, pI, aliphatic index (AI), GRAVY, average flexibility (AF), and average disorder (AD)) to PC1 and PC2. All variables contribute similarly to PC1, whereas PC2 is dominated by ΔG° and pI, whose vectors point in opposite directions. This inverse relationship indicates that higher pI (greater basicity) is associated with more favorable ΔG° values (stronger binding), consistent with the thermodynamic interpretation. Numerical values of the scores and loadings are available in the Appendix.*

a net negative charge at pH 7. This charge complementarity suggests that electrostatic attraction may contribute significantly to the interaction between dystrophin and DBNa-CC. In contrast, DBNb-CC, DBNb-CC-NTM, and DBNb-CC-CTM have predicted pI values in the acidic to near-neutral range (**Table 1**). As a result, these constructs do not exhibit the same electrostatic advantage for binding to dystrophin, implying that their interactions may rely more heavily on specific polar contacts, hydrogen bonding, or structural complementarity rather than overall charge complementarity.

Our PCA results are shown in **Figure 3**. PCA reduced the dimensionality of the dataset from six variables to two principal components, with PC1 and PC2 together explaining 99.5% of the total variance. This substantial dimensional reduction enables a straightforward visual and quantitative assessment of the relationships among the dystrobrevin variants, which can be represented on a two-dimensional score plot (**Figure 3a**).

The score plot reveals that the first principal component (PC1) distinguishes the two dystrobrevin isoforms: DBNa-CC and DBNb-CC. The N-terminal mutant of DBNb-CC (DBNb-CC-NTM) shows minimal deviation from the native DBNb-CC along PC1, whereas the C-terminal mutant (DBNb-CC-CTM) exhibits a marked shift along PC1. This suggests that the C-terminal flanking region has a greater influence on the physicochemical properties most relevant to dystrophin binding.

The corresponding loadings plot (**Figure 3b**) quantifies the contribution of $\Delta G°$ and the five bioinformatic variables to PC1 and PC2. All six variables contribute to PC1 with similar magnitude, indicating that PC1 reflects a composite of multiple physicochemical differences among the constructs. In contrast, PC2 is dominated primarily by $\Delta G°$ and pI, whose loading vectors point in opposite directions. This inverse relationship indicates that as pI increases (i.e., the construct becomes more basic), $\Delta G°$ becomes more negative, corresponding to stronger binding affinity—a finding consistent with our thermodynamic interpretation.

Our primary objective was to evaluate whether $\Delta G°$ can be predicted from intrinsic sequence-derived properties. To address this question, we applied multiple linear regression (Roustaei, 2024). Because only four observations were available (the four dystrobrevin variants), a maximum of two predictor variables could be included in the model. Based on their correlations with $\Delta G°$ (**Table 2**), the two most informative variables—pI and AD—were selected as predictors.

Multiple linear regression using Eq. (3) yielded the following relationship:

$$\Delta G° = -0.793\ \mathrm{pI} - 11.664\ \mathrm{AD} + 4.741 \qquad (4)$$

Table 1. *Bioinformatic variables used in principal component analysis (PCA). The five computed properties for each dystrobrevin construct are: isoelectric point (pI), aliphatic index (AI), grand average of hydropathy (GRAVY), average flexibility (AF), and average disorder (AD).*

Dystrobrevin	pI	AI	GRAVY	AF	AD
DBNa-CC	8.09	90.37	-0.928	0.4534	0.5682
DBNb-CC	5.5	82.28	-1.113	0.4503	0.6382
DBNb-CC-NTM	5.49	86.58	-1.039	0.4519	0.6100
DBNb-CC-CTM	7.23	85.79	-1.036	0.4514	0.6001

Table 2. *Correlation matrix among ΔG° and the five bioinformatic variables used in PCA and regression analysis. Values represent Pearson correlation coefficients.*

	ΔG°	pI	AI	GRAVY	AF	AD
ΔG°	1.0					
pI	-0.938	1.0				
AI	-0.566	0.762	1.0			
GRAVY	-0.648	0.841	0.988	1.0		
AF	-0.496	0.724	0.993	0.982	1.0	
AD	0.743	-0.889	-0.972	-0.988	-0.948	1.0

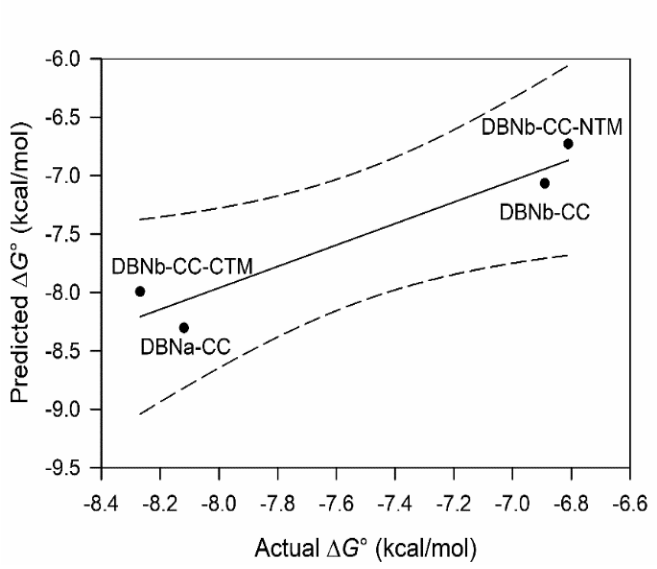

Figure 4. *Multiple linear regression of sequence-derived variables predicts dystrophin–dystrobrevin binding free energy. Predicted versus experimentally measured standard free energy changes (ΔG°) for the four dystrobrevin constructs. The regression model used pI and AD as predictors, yielding the relationship, ΔG° = –0.793pI – 11.664 AD + 4.741. The solid line shows the best-fit regression, and the dashed lines indicate the 95% confidence interval. A strong correlation (R^2 = 0.919) demonstrates that ΔG° can be reliably predicted from sequence-derived properties. All four variants—DBNa-CC, DBNb-CC, DBNb-CC-NTM, and DBNb-CC-CTM—fall within the confidence bounds, validating the model despite the small dataset.*

Model performance was evaluated by comparing predicted and experimentally measured ΔG° values (**Figure 4**). The regression demonstrated a strong correlation between predicted and observed values (R^2 = 0.919), and all four data points fell within the 95% confidence interval, indicating that the model captures the major determinants of ΔG° within this limited dataset. Given the small dataset (n = 4), this model should be considered exploratory and intended to guide future experimental screening rather than serve as a definitive predictive tool.

4. Discussion

Dystrophin plays an essential role in maintaining neuronal structure and synaptic function, in part through its interactions with dystrobrevin and other components of the dystrophin-associated protein complex (Tetorou et al., 2025). For example, loss of dystrophin disrupts inhibitory signaling and contributes to cognitive impairment and seizures in Duchenne muscular dystrophy (Naidoo & Anthony, 2020; Sekiguchi et al., 2009). Therefore, identifying additional binding partners of dystrophin is an important step toward understanding its broader roles in the nervous system.

In this study, we examined dystrophin–dystrobrevin interactions using a combined framework of thermodynamics and bioinformatics. Our thermodynamic analysis showed that binding is driven primarily by enthalpically favorable electrostatic and polar interactions, whereas entropic contributions are unfavorable. This trend is consistent with the charge complementarity observed between dystrophin and DBNa-CC. Importantly, we demonstrated EEC across the four dystrobrevin constructs. The presence of EEC suggests that dystrophin may accommodate a range of binding partners through compensating energetic contributions—a thermodynamic hallmark often associated with binding promiscuity (Kang & Smidtas, 2021). The unusually low compensation temperature observed here may reflect the intrinsic rigidity of coiled-coil structures, although further structural investigations are warranted.

Our bioinformatic and multivariate analyses provided additional insight into the determinants of binding specificity. PCA effectively separated the two dystrobrevin isoforms and revealed that the C-terminal flanking region contributes substantially to the physicochemical properties relevant to dystrophin binding, illustrating the usefulness of PCA in biomedical research (Bouldin et al., 2024; Higdon & Kang, 2024; Kang & Patterson, 2011; Negron et al., 2024; Negron & Kang, 2025). Loadings analysis highlighted pI as one of the strongest contributors to $\Delta G°$, reinforcing the importance of electrostatics in modulating affinity. Multiple linear regression further demonstrated that $\Delta G°$ can be predicted from sequence-derived variables—particularly pI and AD—suggesting that sequence-based models may help identify new dystrophin-binding proteins across the proteome.

Together, these results provide a thermodynamic rationale for the broad interaction capacity of dystrophin and offer a computational framework for narrowing potential binding partners in the nervous system. Future work integrating thermodynamic, structural, and proteomic approaches may help illuminate the full scope of dystrophin's interactome and its relevance to Duchenne muscular dystrophy-associated neurological symptoms.

Conflict of Interest Statement

The authors declare no conflict of interest.

Appendix

*Numerical values in the score plot (**Figure 3a).***

Observation	PC1	PC2
DBNa-CC	2.897	0.220
DBNb-CC	-2.558	-0.193
DBNb-CC-NTM	-0.704	1.048
DBNb-CC-CTM	0.365	-1.076

*Numerical values in the loadings plot (**Figure 3b**).*

Variable	PC1	PC2
Free energy	-0.774	0.628
pI	0.918	-0.378
AI	0.956	0.286
GRAVY	0.984	0.176
AF	0.933	0.359
AD	-0.997	-0.0525

References

Benson, M.A., Newey, S.E., Martin-Rendon, E., Hawkes, R. *et al*. (2001) Dysbindin, a novel coiled-coil-containing protein that interacts with the dystrobrevins in muscle and brain. *Journal of Biological Chemistry* **276**, 24232–24241.

Bouldin, R.C., Higdon, J.R. & Kang, J. (2024) Quantitative analysis of the effects of acoustic neurostimulation on the neuropsychology of healthy adults. *Exploration of Neuroprotective Therapy* **4**, 319–324.

Chang, R. (2005) *Physical Chemistry for the Biosciences*. Mill Valley, CA. University Science Books.

Dang, V., Voigt, B. & Marcotte, E.M. (2025) Progress toward a comprehensive brain protein interactome. *Biochemical Society Transactions* **53**, 303–314.

Daune, M. (1999) *Molecular Biophysics: Structures in Motion*. New York. Oxford University Press.

Durrani, M.K. & Kang, J. (2020) Thermodynamic analysis of the binding of p38 MAPK to substrate proteins. *Journal of Biological Chemistry* **295**, 1366.

Fox, J.M., Zhao, M., Fink, M.J., Kang, K., et al. (2018) The molecular origin of enthalpy/entropy compensation in biomolecular recognition. *Annual Review of Biophysics* **47**, 223–250.

Griessen, R. & Dam, B. (2021) Simple accurate verification of enthalpy-entropy compensation and isoequilibrium relationship. *Chemphyschem* **22**, 1774–1784.

Higdon, J.R. & Kang, J. (2024) Principal component analysis on the effect of early morning awakening in major depressive disorder. *Journal of Multiscale Neuroscience* **3**, 94–97.

Howes, O., Marcinkowska, J., Turkheimer, F.E., *et al*. (2025) Synaptic changes in psychiatric and neurological disorders: state-of-the-art of in vivo imaging. *Neuropsychopharmacology* **50**, 164–183.

Kang, J. & Auerbach, J.D. (2009) Thermodynamic characterization of dissociation rate variations of human leukocyte antigen and peptide complexes. *Molecular Immunology* **46**, 2873–2875.

Kang, J. & Kang, A.M. (2021) Statistical and thermodynamic analysis of the binding of trans-activation response-binding proteins to HIV-1 TAR RNA. *Journal of Biological Chemistry* **296**, 100067.

Kang, J. & Patterson, A. K. (2011) Principal component analysis of mRNA levels of genes related to inflammation and fibrosis in rats treated with TNBS or glutamine. *Inflammatory Bowel Diseases* **17**, 1630–1631.

Kang, J. & Smidtas, L. (2021) Enthalpy–entropy compensation in the binding of peptide ligands to human Arc. *Biochemical and Biophysical Reports* **27**, 101088.

Kragelj, J., Orand, T., Delaforge, E. *et al.* (2021) Enthalpy–entropy compensation in the promiscuous interaction of an intrinsically disordered protein with homologous protein partners. *Biomolecules* **11**, 1204.

Mathew, B., Wang, H., Tran, T., Li, Y. *et al.* (2022) Deciphering spatial protein–protein interactions in brain using proximity labeling. *Molecular & Cellular Proteomics* **21**, 100422.

Matsubayashi, J. & Takano, T. (2025) Proximity labeling uncovers the synaptic proteome under physiological and pathological conditions. *Frontiers in Cellular Neuroscience* **19**, 1638627.

Naidoo, M. & Anthony, K. (2020) Dystrophin Dp71 and the neuropathophysiology of Duchenne muscular dystrophy. *Molecular Neurobiology* **57**, 1748–1767.

Negron, D.E., Higdon, J.R. & Kang, J. (2024) Metabolomic distance between normal and obese children. *Steroids* **208**, 109451.

Negron, D.E. & Kang, J. (2025) Comment on "Monoclonal antibodies engineered with Fc region mutations to extend protection against fentanyl toxicity". *The Journal of Immunology* **214**, 1434–1435.

Pardoe, I. (2012) *Applied Regression Modeling*. 2nd Ed. Wiley, Hoboken, New Jersey.

Payá, G., Bautista, V., Camacho, M., Esclapez, J. *et al.* (2023) Comprehensive bioinformatics analysis of the biodiversity of Lsm proteins in the Archaea domain. *Microorganisms* **11**, 1196.

Peters, M. F., Adams, M. E. & Froehner, S. C. (1997) Differential association of syntrophin pairs with the dystrophin complex. *Journal of Cell Biology* **138**, 81–93.

Roberts, R. G. (2001) Dystrophins and dystrobrevins. *Genome Biology* **2**, REVIEWS3006.

Roustaei, N. (2024) Application and interpretation of linear-regression analysis. *Medical Hypothesis, Discovery & Innovation in Ophthalmology* **13**, 151–159.

Sekiguchi, M., Zushida, K., Yoshida, M., Maekawa, M. *et al.* (2009) A deficit of brain dystrophin impairs specific amygdala GABAergic transmission and enhances defensive behaviour in mice. *Brain* **132**, 124–135.

Taylor, C. L. Hummert, J. G. & Kang, J. (2023) Enthalpy-entropy compensation in the binding of quercetin to calf thymus DNA. *Journal of Molecular Recognition* **36**, e2994.

Tetorou, K., Aghaeipour, A., Singh, S., Morgan, J.E. et al. (2025) The role of dystrophin isoforms and interactors in the brain. *Brain* **148**, 1081–1098.

Upadhyay, V., Ray, S., Panja, S., Saviola, A. J. *et al.* (2024) Biophysical characterization of the dystrophin C-terminal domain: dystrophin interacts differentially with dystrobrevin isoforms. *Journal of Biological Chemistry* **300**, 108002.